

Computational Investigation of the Concerted Dismutation of Chlorite Ion by Water-Soluble Iron Porphyrins

Jason M. Keith,^{*,†,‡} Mahdi M. Abu-Omar,[§] and Michael B. Hall^{*,‡}

[†]Theoretical Division, MS B268, Los Alamos National Laboratory, Los Alamos, New Mexico 87545, United States

[‡]Department of Chemistry, Texas A&M University, College Station, Texas 77843, United States

[§]Brown Laboratory, Department of Chemistry, Purdue University, 560 Oval Drive, West Lafayette, Indiana 47907, United States

S Supporting Information

ABSTRACT: A detailed density functional theory examination of the reaction of an iron porphyrin chlorite dismutase model complex with chlorite was performed. We find that the molecular oxygen production observed occurs via the formation of η^1 -Fe(III) chlorite species, followed by the formation of O=Fe(IV) (compound II) and chlorine monoxide through homolytic bond cleavage. Chlorine monoxide then rebounds to form Fe(III)-peroxyhypochlorite followed by subsequent loss of chloride and loss of dioxygen accompanied by spin conversion to produce the Fe(III) complex and complete the catalytic cycle.

Contamination of the water supply by oxychlorine anions (ClO_x^-) is a potential threat to human health and the environment.¹ These chemicals are widely produced for use as explosives,² bleaching agents,³ herbicides,⁴ and disinfectants.⁵ As a result, the use of redox and decomposition reactions to reduce ClO_x^- in the environment is of great interest.

Of particular interest are perchlorate-respiring bacteria, which possess two enzymes that reduce ClO_x^- species, perchlorate reductase, which reduces perchlorate to chlorate and chlorate to chlorite,⁶ and chlorite dismutase (Cld), which reduces chlorite to chloride and produces O_2 .⁷

Recently, Zdilla et al. developed several water-soluble Fe porphyrins as functional models for Cld (Figure 1).⁸ These complexes react with ClO_2^- via two competing pathways. One leads to the formation of O_2 and Cl^- , similar to Cld, and the other to the formation of ClO_3^- .⁹ While all three complexes are competent at producing O_2 , A is more efficient with 18% yield of O_2 compared to 3 and 7% yield for B and C. Yield of ClO_3^- varies accordingly, with values of 56, 63, and 62%.

To rationalize the formation of O_2 by the first pathway mentioned above, the authors propose three mechanisms (Scheme 1). All three mechanisms begin with the addition of ClO_2^- to Fe(III) to form a Fe(III)- ClO_2 adduct. Mechanism i then proceeds through loss of ClO^- to form the O=Fe^{IV}(Por^{•+}) intermediate (compound I), followed by reaction with $[\text{ClO}_n]^-$ ($n = 1, 2$) to form $[\text{ClO}_{n-1}]^-$ and molecular oxygen. Mechanisms ii and iii form O_2 from the O atoms from the same chlorite molecule. Mechanism ii proceeds via a rebound step through which ClO^- is not released into solution but reacts to form an Fe(III)-OOCl that subsequently loses Cl^- and O_2 . Mechanism iii proceeds through a Cl migration to form the same peroxyhypochlorite intermediate. In an effort to distinguish between these

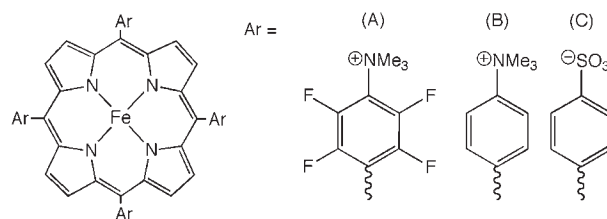
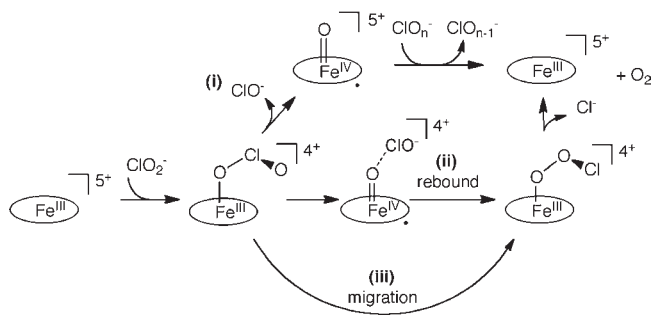


Figure 1. Structure of Fe(III) porphyrin model complexes.¹⁰

Scheme 1. Possible Mechanistic Pathways for O_2 Formation



mechanisms, Zdilla et al. performed a series of reactions with ^{18}O -labeled chlorite and ^{16}O -water (solvent) and concluded that the O atoms in each O_2 , formed originated from the same ClO_2^- molecule (i.e., no crossover), thus ruling out mechanism i as a route to O_2 formation.⁸

While pathway i was successfully ruled out as a pathway for dioxygen production, Zdilla et al. did find that the formation of the O=Fe^{IV}(Por^{•+}) intermediate (compound I) leads to the production of chlorate through reaction with another chlorite molecule.⁸

In an effort to differentiate the rebound and migration mechanisms for molecular oxygen formation, we present herein a detailed density functional theory (DFT) examination of the potential energy surface for the reaction of chlorite with a 5,10,15,20-tetrakis-porphyrin model complex (Figure 2).

All calculations were unrestricted DFT calculations performed with the hybrid functional B3LYP,^{11,12} as implemented by the Gaussian09 program package.¹³ This functional is known to produce good descriptions of geometries and reaction profiles

Received: May 9, 2011

Published: August 01, 2011

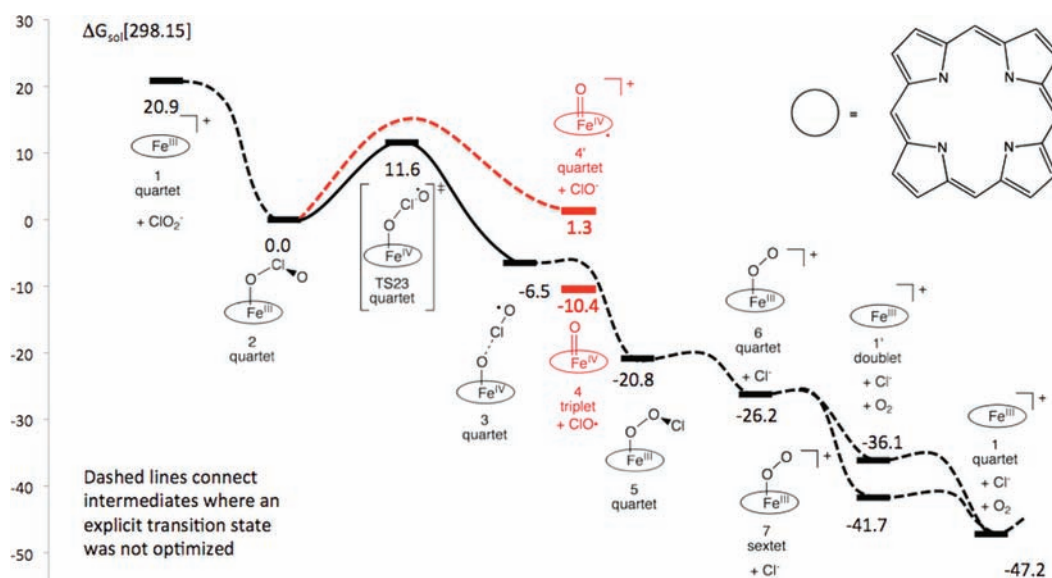


Figure 2. Potential energy surface for the formation of O_2 from ClO_2^- by the Fe(III) model complex (see further discussion in the SI).

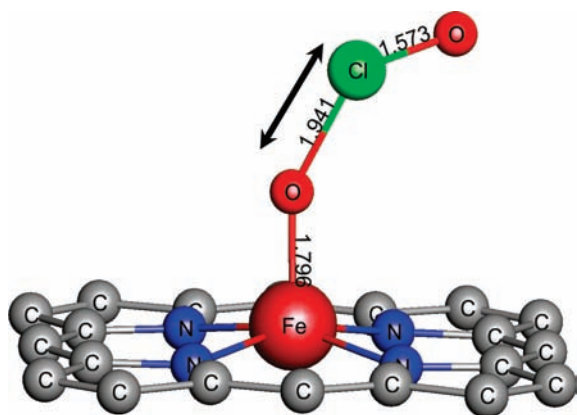


Figure 3. Structure for Cl–O bond cleavage (TS23).

for transition-metal-containing compounds.¹⁴ Fe was modeled with the LANL2DZ effective core potential and basis set,¹⁵ with the 4p orbitals replaced with the split valence functions from Couty and Hall.¹⁶ All other atoms were modeled using a Pople style¹⁷ double- ζ 6-31G(d',p') basis set with polarization functions optimized for heavy atoms.¹⁸ The doublet, quartet, and sextet spin states were examined for all species with an odd number of electrons, and spin densities were examined for validation. The ground-state species for the starting Fe(III) complex was found to be the quartet, in agreement with experimental observation.

All geometries were evaluated for the correct number of imaginary frequencies using the analytical Hessian. Zero point energies as well as enthalpy and entropy corrections for 298.15 K were also calculated and added to the total energy to obtain a total free energy, $\Delta G[298.15]$.

Implicit solvent effects were incorporated using the polarizable continuum model¹⁹ with radii and nonelectrostatic terms from Truhlar and co-workers' SMD solvation model²⁰ for water using the parameter $\epsilon = 75.3553$. The solvent effects were calculated at geometries calculated in the gas phase, resulting in a solution-phase free energy.

Binding chlorite to Fe(III), **1**, was found to be exergonic with $\Delta G_{\text{sol}} = -20.9$ kcal/mol and resulted in an Fe(III)-chlorite intermediate, **2**. Chlorite is bound to the Fe(III) center in an η^1 fashion by O with a bond distance of 1.97 Å (with Fe–O_{unbound} distance = 3.8 Å), while the Fe atom has shifted slightly out of the plane of the porphyrin (trans N–Fe–N angle = 165°). The Fe–O–Cl–O dihedral angle is $\sim 70^\circ$. The two O–Cl bond distances are 1.67 Å (bound to Fe) and 1.56 Å (unbound) compared to a distance of 1.62 Å in free ClO_2^- .

From species **2**, the reaction was found to proceed via a homolytic bond cleavage to produce $\text{ClO}\cdot$ and $\text{O}=\text{Fe}(\text{IV})$ (compound **II**) in a loosely bound van der Waals complex, **3** ($\Delta G_{\text{sol}} = -6.5$ kcal/mol). The connecting transition state, TS23, $\Delta G_{\text{sol}}^\ddagger = 11.6$ kcal/mol, exhibits a decreasing Fe–O distance of 1.80 Å and an increasing O_{bound}–Cl distance of 1.94 Å (compared to 2.72 Å in **3**), and the imaginary frequency corresponds primarily to the Cl–O_{bound} stretch (Figure 3). A Mulliken spin density of 0.53 electrons on the Cl–O_{unbound} moiety shows partial radical character in TS23, and there is a full electron on the chlorine monoxide moiety in the product **3** (0.78 electrons on O and 0.22 electrons on Cl).

From **3**, the loss of chlorine monoxide to solution is downhill by 3.9 kcal/mol to form species **4**; however, chlorine monoxide can rebound to form Fe(III)-peroxyhypochlorite, **5**, which is energetically favorable by 14.3 kcal/mol. This rebound occurs by simply rotating the chlorine monoxide by $\sim 90^\circ$. While a transition state for this process was not located, the enthalpy cost of 1.5 kcal/mol for the complete removal of chlorine monoxide to form **4** can be used as an upper bound for this process (i.e., assuming all of the enthalpic penalty without any of the entropic gain from $\text{ClO}\cdot$ loss).

From **5**, the loss of chloride to form species **6** and subsequent release of molecular oxygen with an accompanying spin conversion completes the catalytic cycle by producing species **1** with an overall $\Delta G_{\text{sol}} = -68.1$ kcal/mol.

In contrast to this chlorine monoxide rebound process, the formation of hypochlorite and $\text{O}=\text{Fe}^{\text{IV}}(\text{Por}^{\bullet+})$ (compound **I**), **4'**, through heterolytic bond cleavage was considered and the products were found to be 11.7 kcal/mol higher in energy than **4**. Spin density examination of species **4'** shows that there is a single unpaired spin on the porphyrin ring as observed experimentally.

Table 1. Relative Energies for Complexes A and B

complex	2	4	4'
A	0.0	-15.4	6.5
B	0.0	-13.7	2.1

4' is approximately isoenergetic with 2 with $\Delta G_{\text{sol}} = 1.3$ kcal/mol relative to 2. In addition, we speculate that hypochlorite, being less reactive than chlorine monoxide, would be less likely to rebound. Thus, the formation of 4' results in the release of hypochlorite and the resulting $\text{O}=\text{Fe}^{\text{IV}}(\text{Por}^{\bullet+})$ (compound I), which leads to the formation of chlorate, as observed experimentally by Zdilla et al.⁸

In addition to examination of the rebound mechanism, an Cl migration/O insertion process was examined to go from 2 directly to 5 in a concerted step. After standard transition-state methods failed, two one-dimensional relaxed scans of the potential energy surface near species 2 were performed; one examined the energy as a function of the O–O distance, while the other examined the energy as a function of the O–Cl–O angle. In both instances, a local maximum was located with an elongated Cl–O_{bound} distance. Optimization of these potential saddle points converged to the homolytic bond cleavage transition state TS23, suggesting that a concerted process is not at work.

In order to test the homolytic bond cleavage/rebound mechanism hypothesis with the actual ligands, species 2, 4, and 4' were examined for complexes A and B (Table 1). The resulting free energies show that species 4 is 1.7 kcal/mol more stable with respect to 2 for complex A than B, while the converse is true for species 4' ($\Delta\Delta G_{\text{sol}} = 4.4$ kcal/mol). We suggest that the electron-withdrawing fluorine atoms make the porphyrin ligand less susceptible to oxidation, which simultaneously stabilizes 4 and destabilizes 4'. Again, this is consistent with the results of Zdilla et al. because complex A produced more O₂ and less ClO₃⁻ than B.⁸

In conclusion, we have performed a detailed DFT examination of the reaction of Fe(III)-porphyrin with ClO₂⁻ as a model for the Cl_d enzyme models developed by Zdilla et al.⁸ We find that the O₂ production observed occurs via the formation of η^1 -Fe(III)-chlorite species, followed by the formation of $\text{O}=\text{Fe}(\text{IV})$ (compound II) and ClO· through homolytic bond cleavage. ClO· then rebounds to form an Fe(III)-OOCl followed by the subsequent loss of Cl⁻ and loss of O₂ accompanied by spin conversion to produce the Fe(III) complex and complete the catalytic cycle. Through this examination, we have been able to rule out the possibility of a concerted oxygen migration mechanism. In addition, we point to the competitive heterolytic bond cleavage process producing ClO⁻ and $\text{O}=\text{Fe}^{\text{IV}}(\text{Por}^{\bullet+})$ (compound I) as the source of observed ClO₃⁻, consistent with the experimental findings of Zdilla et al.⁸ To further emphasize the legitimacy of these results, the products of both the homolytic, species 4, and heterolytic, species 4', bond cleavage reactions were examined for $[\text{Fe}(\text{TF}_4\text{TMAP})]^{5+}$, A, and $[\text{Fe}(\text{TMAP})]^{5+}$, B, and compared to the respective bound ClO₂⁻ species. It was demonstrated that A favors homolytic bond cleavage with respect to B while disfavoring heterolytic bond cleavage. Again, this is consistent with the observed reactivity of A and B by Zdilla et al.⁸

■ ASSOCIATED CONTENT

S Supporting Information. Additional discussion of the potential energy surface in Figure 2, E, H, and G data for all species, basis set from genecp, and geometries for all species. This material is available free of charge via the Internet at <http://pubs.acs.org>.

■ AUTHOR INFORMATION

Corresponding Author

*E-mail: jkeith@lanl.gov (J.M.K.), hall@science.tamu.edu (M.B.H.).

■ ACKNOWLEDGMENT

J.M.K. and M.B.H. acknowledge support of The Welch Foundation (Grant A-0648). J.M.K. acknowledges LANL Director's Postdoctoral Fellowship. The Los Alamos National Laboratory is operated by Los Alamos National Security, LLC, for the National Nuclear Security Administration of the U.S. Department of Energy under Contract DE-AC5206NA25396.

■ REFERENCES

- (1) (a) USEPA. National Primary Drinking Water Regulations; Disinfectants and Disinfection Byproducts Notice of Data Availability; Proposed Rule. *Fed. Regist.* **1998**, *63*, 15674. (b) USEPA. Priority List of Substances Which May Require Regulation under the Safe Drinking Water Act. *Fed. Regist.* **1991**, *56*, 1470. (c) *Drinking Water and Health*; Boraks, J., Ed.; National Research Council, National Academy Press: Washington, DC, 1987; pp 99–111. (d) Rosmarin, A.; Lehtinen, K.-J.; Notini, M.; Mattsson, J. *Environ. Pollut.* **1994**, *85*, 3. (e) van Wijk, D. J.; Hutchingson, T. H. *Ecotoxicol. Environ. Saf.* **1995**, *32*, 244. (f) Lehtinen, K.-J.; Notini, M.; Mattsson, J.; Lander, L. *Ambio* **1998**, *17*, 387.
- (2) Hogue, C. *Chem. Eng. News* **2003**, *81*, 127.
- (3) (a) Axegård, P.; Gunnarsson, L.; Malmqvist, A. *Sven. Papperstidn.* **1989**, *92*, 50. (b) Germgård, U.; Tder, A.; Tormund, D. *Pap. Puu* **1981**, *63*, 127.
- (4) Åslander, A. *J. Agric. Res.* **1928**, *36*, 915.
- (5) Harman, D. C.; Frankenberger, W. T. *J. Environ. Qual.* **1999**, *28*, 1018.
- (6) (a) Kengen, S. W. M.; Rikken, G. B.; Hagen, W. R.; van Ginkel, C. G.; Stams, A. J. M. *J. Bacteriol.* **1999**, *181*, 6706. (b) Okeke, B. C.; Frankenberger, B. W. T. *Microbiol. Res.* **2003**, *158*, 337. (c) Bender, K. S.; Shang, C.; Cakraborty, R.; Belckik, S. M.; Coates, J. D.; Achenback, L. A. *J. Bacteriol.* **2005**, *187*, 5090.
- (7) (a) van Ginkel, C. G.; Rikken, G. B.; Kroon, A. G. M.; Kengen, S. W. M. *Arch. Microbiol.* **1996**, *166*, 321. (b) Stencklo, K.; Thorell, H. D.; Bergius, H.; Aasa, R.; Nilsson, T. *J. Biol. Inorg. Chem.* **2001**, *6*, 601. (c) Xu, J.; Logan, B. E. *J. Microbiol. Methods* **2004**, *271*, 3539. (d) Bender, K. S.; O'Connor, K. S. A.; Cakraborty, R.; Coates, J. D.; Achenback, L. A. *Appl. Environ. Microbiol.* **2002**, *68*, 4820. (e) Lee, A. Q.; Streit, B. R.; Zdilla, M. J.; Abu-Omar, M. M.; DuBois, J. L. *Proc. Natl. Acad. Sci. U.S.A.* **2008**, *105*, 15654.
- (8) (a) Zdilla, M. J.; Lee, A. Q.; Abu-Omar, M. M. *Angew. Chem., Int. Ed.* **2008**, *47*, 7697. (b) Zdilla, M. J.; Lee, A. Q.; Abu-Omar, M. M. *Inorg. Chem.* **2009**, *48*, 2260.
- (9) The overall thermodynamics are -35.6 and -45.2 kcal/mol, and this enzyme is selective for the unfavorable product (from ref 8b).
- (10) $[\text{Fe}(\text{TF}_4\text{TMAP})][\text{OTf}]_s$, A; $[\text{Fe}(\text{TMAP})][\text{Cl}]_s$, B; $[\text{Na}]_3$ - $[\text{Fe}(\text{TPPS})]$, C. TF₄TMAP = 5,10,15,20-tetrakis(2,3,5,6-tetrafluoro-4-N,N-trimethylanilinium)porphyrin; TMAP = 5,10,15,20-tetrakis(4-N,N-trimethylanilinium)porphyrin; TPPS = 5,10,15,20-tetrakis(4-sulfonato-phenyl)porphyrin.
- (11) Becke, A. D. *J. Chem. Phys.* **1993**, *98*, 5648.
- (12) Lee, C.; Yang, W.; Parr, R. G. *Phys. Rev. B* **1988**, *37*, 785.
- (13) Frisch, M. J.; et al. *Gaussian09*, revision B.01; Gaussian, Inc.: Wallingford, CT, 2009.
- (14) Niu, S.; Hall, M. B. *Chem. Rev.* **2000**, *100*, 353.
- (15) Hay, P. J.; Wadt, W. R. *J. Chem. Phys.* **1985**, *82*, 299.
- (16) Couty, M.; Hall, M. B. *J. Comput. Chem.* **1996**, *17*, 1359.
- (17) (a) Hariharan, P. C.; Pople, J. A. *Chem. Phys. Lett.* **1972**, *16*, 217. (b) Francl, M. M.; Pietro, W. J.; Hehre, W. J.; Binkley, J. S.; Gordon, M. S.; DeFrees, D. J.; Pople, J. A. *J. Chem. Phys.* **1982**, *77*, 3654.
- (18) Krishnan, R.; Binkley, J. S.; Seeger, R.; Pople, J. A. *J. Chem. Phys.* **1980**, *72*, 650.
- (19) Tomasi, J.; Mennucci, B.; Cammi, R. *Chem. Rev.* **2005**, *105*, 2999.
- (20) Marenich, A. V.; Cramer, C. J.; Truhlar, D. G. *J. Phys. Chem. B* **2009**, *113*, 6378.